UNIVERSITY OF CALIFORNIA,
IRVINE

Development of Diffuse Optical Spectroscopic Imaging (DOSI) for Quantitative Determination of Body Composition

THESIS

submitted in partial satisfaction of the requirements
for the degree of

MASTER OF SCIENCE

in Biomedical Engineering

by

Drew Reilly

Thesis Committee:
Professor Bruce J. Tromberg, Chair
Professor Vasan Venugopalan
Professor Michelle A. Digman

2017

DEDICATION

To

January and Kevin

Thank you for all you have done, and all you continue to do for me.

Wubba lubba dub dub

Rick Sanchez
"Rick and Morty"

TABLE OF CONTENTS

LIST OF FIGURES

LIST OF EQUATIONS

LIST OF TABLES

LIST OF SYMBOLS/ABBREVIATIONS

Symbol	Meaning
μ_a	Absorption Coefficient
μ_s'	Reduced Scattering Coefficient
λ	wavelength
A_s	Scattering Amplitude
b_s	Scattering Power
R	Measured Reflectance
A	Reflectance Amplitude
C_0	Instrument Amplitude
phi	Reflectance Phase
phi_0	Instrument Phase
e	Euler's number
i	Square root of negative one
THI_{BB}	Broadband Tissue Hydration Index
THI_{SS}	Steady State Tissue Hydration Index

Abbreviations	Meaning
DOSI	Diffuse Optical Spectroscopic Imaging
DXA	Dual Energy X-ray Absorptiometry
MRI	Magnetic Resonance Imaging
CT	Computerized Tomography
THI	Tissue Hydration Index
BS	Short Head of Bicep
BL	Long Head of Bicep
GL	Lateral Gastrocnemius
GM	Medial Gastrocnemius
LL	Lower Left Abdomen
LR	Lower Right Abdomen
RF	Rectus Femoris
SM	Middle Shin
SU	Upper Shin
UL	Upper Left Abdomen
UR	Upper Right Abdomen
VL	Vastus Lateralus

ACKNOWLEDGMENTS

I would like to express the deepest appreciation to my committee chair, Professor Bruce J. Tromberg, whose intelligence is exceeded only by his patience with me. Without his guidance and persistent help this dissertation would not have been possible.

I would like to thank my committee members, Professor Vasan Venugopalan and Professor Michelle A. Digman, whose works have demonstrated to me the full scope of biophotonics.

I would like to thank all members of the DOSI lab, who have helped me tremendously over the past two years. This includes, but is not limited to, Amanda Durkin, Anais Leproux, Brian Hill, Hossein Yazdi, and Jesse Lam. And special thank you to Robert Warren, without whom this work would not have been possible.

ABSTRACT OF THE THESIS

Development of Diffuse Optical Spectroscopic Imaging (DOSI) for Quantitative Determination of Body Composition

By

Drew Reilly

Master of Science in Biomedical Engineering

University of California, Irvine, 2017

Professor Bruce J. Tromberg, Chair

Body composition and tissue hydration are critical parameters that play an essential role in each person's health status and disease risk. Current techniques for accurately and quantitatively measuring these features either lack sensitivity or are difficult and expensive to operate. Here, I present a new method for evaluating body composition using Diffuse Optical Spectroscopy. I also introduce a Tissue Hydration Index (THI), a method to assess the relative water content or hydration status of a person's tissue. THI is developed using DOSI technology and a simplified approach for deriving the index using time-independent spectroscopy is proposed and validated.

INTRODUCTION

For at least 30 years, obesity and overweight has become more prevalent throughout the world, with increased prevalence seen in developed and undeveloped countries, in children and adults, and both sexes (Ng et al. 2014). Obesity is associated with many additional health issues (Lavie et al. 2009), shortens lifespan (PSC et al. 2009), and represents excessive personal, industrial, and societal monetary costs (Loeppke et al. 2009, Tsai et al. 2011). In addition to the need for better prevention and treatment of obesity, enhanced screening and monitoring techniques could play a role in optimizing such prevention and treatment methods. For example, body mass index (BMI) has been used for over 100 years to characterize an individual's body fatness, but it is only an estimate of adiposity. Direct methods to assess body composition involve cadaver analysis, but indirect methods, such as hydrodensitometry or dual energy x-ray absorptiometry (DXA), have been developed which involve some form of assumption about biological tissues. Unfortunately, these more accurate methods to determine adiposity are typically not portable and cannot be accessed by large portions of the population. Magnetic Resonance Imaging (MRI) and Computed Tomography (CT) are the most accurate devices for quantifying body composition, but are expensive and time consuming and, in the case of CT, expose patients to ionizing radiation. In addition to these restrictions, direct body composition assessment methods may not be able to measure obese patients due to size restrictions.

In addition to body composition, there is significant interest in assessing tissue water content or hydration status. Tissue water content measurements during exercise have shown that dehydration can impact mental and physical status (Mudambo et al.

1997). Tissue water content imbalances are associated with many diseases, including but not limited to high blood pressure, obesity, muscle cramps, and digestion problems (Sarvazyan et al. 2005). MRI is the best measurement tool available, but still has all the limitations listed above. Bioelectric impedance methods have been developed to measure tissue water and fat content, but accuracy is variable and only average body values can be determined (Lorenzo et al. 2003). In sports medicine, a field which is heavily interested in hydration and water content measurements, urine and blood tests are often used to measure hydration. But urine tests have limited detection ability and blood tests are invasive and expensive in terms of time and cost (Popowski et al. 2001). Ultrasound assessment of hydration measures changes in soundwaves and associates them with changes in hydration. This allows for excellent indirect monitoring of hydration status of the tissue (Sarvazyan et al. 2005) by visualizing changes in structure and acoustic impedance.

Optics have been used to study water and fat content extensively. One of these optical methods is Diffuse Optical Spectroscopic Imaging (DOSI) is a small, portable, relatively inexpensive tool for measuring concentrations of blood, water and fat. Water and lipid measurements with DOSI have been validated with MRI measurements of emulsion phantoms (Merritt et al. 2003). DOSI breast cancer measurements can separate water into "free" and "bound" states (Chung et al. 2008). In vivo temperature can be measured with DOSI water information (Chung et al. 2010). These studies show that DOSI is a versatile, reliable tool for quantifying tissue water and fat content.

In addition to quantifying water and fat content, optical methods have been used extensively to monitor relative changes in oxygenated hemoglobin and deoxygenated

hemoglobin, as well as tissue oxygen saturation (Elwell et al. 2011). DOSI can go a step further and directly method hemodynamic parameters (Pham et al 2002) as well as quantify absolute concentrations of hemoglobin (Lee et al. 2006).

Here, I present a study using DOSI and DXA to measure a set of healthy young subjects, build a model to measure body composition with DOSI, and introduce a Tissue Hydration Index, a method for measuring tissue hydration using NIRS.

CHAPTER 1: Diffuse Optical Spectroscopy

Diffuse Optical Spectroscopy combines two optical modalities, Frequency Domain Photon Migration (FDPM) and Steady State Broadband Spectroscopy (SS), to fully characterize the optical properties of a turbid tissue (Bevilacqua et al. 2000). Briefly, these optical properties can then be used to determine concentrations of biochemical constituents of tissue. In FDPM, Near Infrared (NIR) laser diodes are intensity modulated at hundreds of megahertz using a radio frequency (RF) source. Light remitted from the tissue is detected by an avalanche photodiode (APD) in contact with the surface. The APD converts the detected light into an RF signal, which is compared to the original RF source to determine the amplitude and phase of the detected light. This process is completed for each laser diode with modulation frequencies typically between 50 - 500 MHz.

In tandem with the FDPM measurement, a SS spectroscopic measurement is taken as well. A Tungsten Halogen lamp is used to illuminate the sample and a broadband reflectance spectrum is recorded. The ability to separate scattering from absorption in the reflectance spectrum is accomplished by processing the FDPM and SS data together.

FDPM data is processed to yield the reduced scattering coefficient (μ_s') and absorption coefficient (μ_a). The measured reflected light (R) is in Equation 1.1.

Equation 1.1: Measured FDPM light

$$R = C_0 * A * e^{-i(phi+phi_0)}$$

A and phi are the modulation amplitude and phase in the FDPM data (Bevilacqua et al. 2000). C_0 and phi_0 are the instrument response coefficients. To obtain C_0 and phi_0, a measurement of optical phantoms with known values for μ_a and μ_s' and every wavelength is taken. Using the known μ_a and μ_s', we compare these to our measured values at our FDPM diode wavelengths to isolate C_0 and phi_0 and remove them from all future measurements. With C_0 and phi_0 known, we apply a nonlinear least squares fit to find A and phi simultaneously. This is done until the function converges and μ_a and μ_s' are known at the FDPM diode wavelengths.

To obtain μ_s' at every wavelength, a power law fit is employed. This method exploits the well-known Mie scattering behavior of light in the range of 650-1000nm in biological tissue and tissue-simulating phantoms (Bevilacqua et al. 2000).. Again, a nonlinear least squares fitting tool is used to find the coefficients to Equation 1.2, where A_S is the "Scattering Amplitude", $b_S$is the "Scattering Slope" and lambda is wavelength.

Equation 1.2 – Power Law Fit of Light Scattering

$$\mu_s'(\lambda) = A_s * \lambda^{-b_s}$$

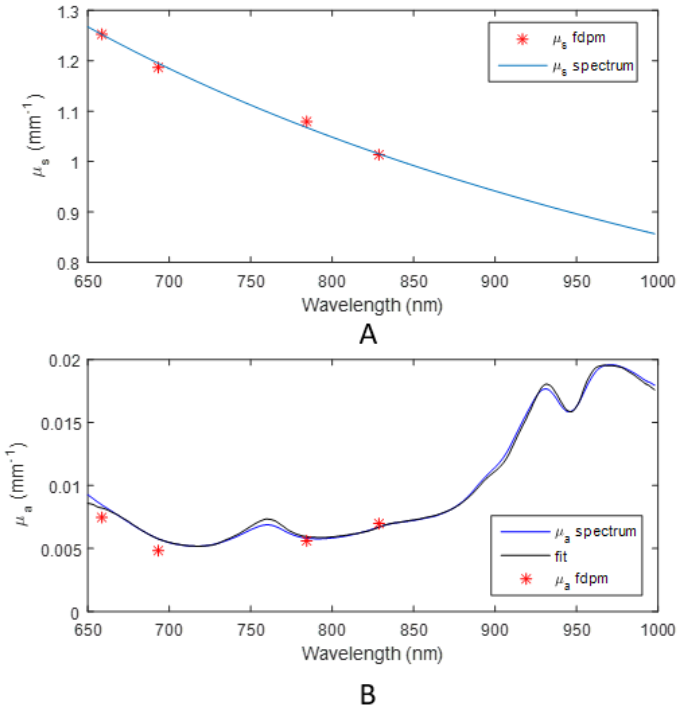

Figure 1.1 – Typical DOSI Measurement on human subject. (A) is the calculated spectrum of the Reduced Scattering Coefficient and (B) is the scatter-corrected tissue absorption spectrum and chromophore fit.

Now that reduced scattering coefficients are known at every wavelength we revisit the steady state measurement. Like with FDPM, a sample of known reflectance is measured to get the instrument response, which is removed from all future measurements. SS measurements at FDPM wavelengths are then scaled by the theoretical reflectance values. From there, the scatter-corrected absorption spectrum is computed by minimizing the difference between the measured and theoretical reflectance values (Figure 1.1).

With the scatter-corrected absorption spectrum computed, a linear least squares method is used to compute chromophore concentrations within the tissue by comparing the measured absorption spectrum with the known spectra for oxy-hemo/myoglobin (HbO2), deoxy-hemo/myoglobin (Hb), water, and lipid. In addition, these parameters are used to compute tissue oxygen saturation (StO2) and total hemo/myoglobin (THbMb).

Previous DOSI Clinical Applications

DOSI has been used in a wide variety of clinical applications. In addition to studies mentioned above, weight loss in obese patients has been shown to change the scattering properties of adipose tissue (Ganesan et al. 2016). The effects of exercise on muscle oxygenation before, during, and after have been studied (Ganesan, Cotter et al. 2015), showing that DOSI is an effective tool for studying muscle tissue. DOSI has been used in many studies to investigate breast cancer. One such study uses the Tissue Optical Index (TOI) to monitor the pathological response in breast cancer tumors during neoadjuvant chemotherapy (O'Sullivan, Leproux et al. 2013).

Dual Energy X-Ray Absorptiometry

In addition to DOSI, Dual Energy X-Ray Absorptiometry (DXA) was used in our study and is considered a gold standard when it comes to body composition measurements (Branski et al 2010). DXA, a whole-body composition assessment tool, uses a three-compartment model to quantify a subject's lean body mass (kg), fat body mass (kg), and body mineral content (kg) by measuring the difference in attenuation between two low energy x-ray beams. DXA measurements were performed with a Hologic Discovery-A DXA system with Apex 3.3 software (Hologic, Marlborough, MA, USA). Prior to scanning, the subject must remove all metal from their person as to not interfere with the measurements.

CHAPTER 2: Body Composition Study

In all, 103 healthy participants aged 7-34 years were measured. While DOSI has been used to study many individuals in the past, measurements on a younger population

such as this are not as common. In addition to using this data set to build the body composition assessment methodologies, optical properties for this population are also reported on which may be of interest to the optics research community.

Table 2.1 – Breakdown of Body Composition Population by Sex

SEX	NUMBER OF SUBJECTS	BMI
FEMALE	54	19.97 ± 3.30
MALE	49	20.23 ± 3.76

Table 2.2 – Breakdown of Body Composition Population by Body Mass Index(BMI) Grouping

BMI	NUMBER OF SUBJECTS
NORMAL	61
OVERWEIGHT	8
UNDERWEIGHT	34

Table 2.3 Breakdown of Body Composition by Age – Sex Grouping.

AGE-SEX GROUPING	NUMBER OF SUBJECTS	BMI
EARLY PUBERTAL BOYS	23	17.71 ± 3.02
EARLY PUBERTAL GIRLS	20	17.52 ± 3.20
LATE PUBERTAL BOYS	18	21.39 ± 2.57
LATE PUBERTAL GIRLS	23	20.17 ± 2.43
ADULT MALES	8	24.86 ± 1.86
ADULT FEMALES	11	22.12 ± 2.29

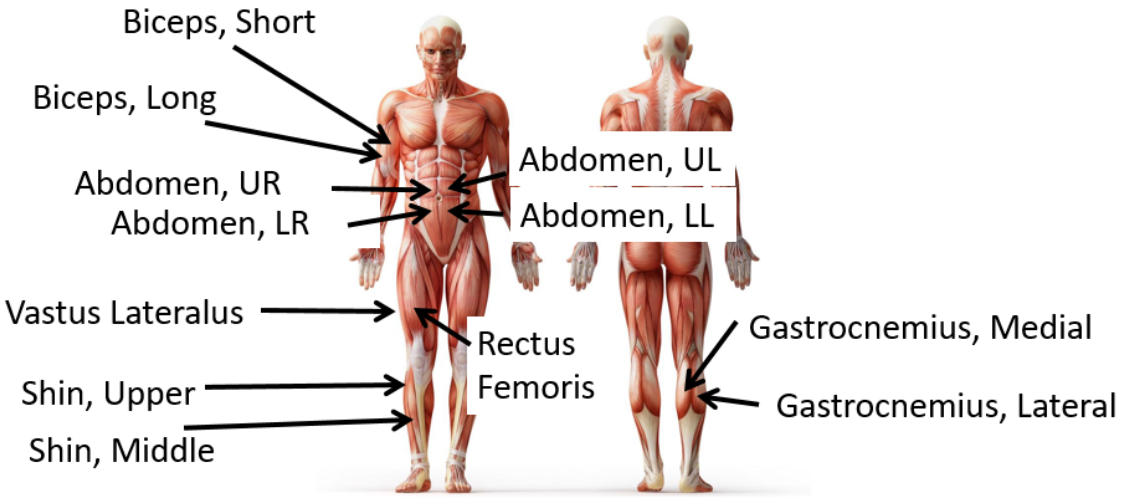

Figure 2.1 – Diagram of DOSI measurement locations on the subject.

DOSI measurements were taken at 12 sites on the body, including two arm, four abdominal, and six leg locations, seen in Figure 2.1. The source-detector separation was set to 28 millimeters for all patient measurements and data was processed using an inhouse MATLAB script. A full body DXA scan was also performed.

The goal of this study was to optical properties for this unique age range and compare the results across groups. Graphs were made along several categories of our sample population. Absorption and scattering parameters (μ_a and μ_s') were plotted for the population separated by sex, age class, sex-age class, and BMI. Age class is a grouping based on three categories: Early Pubertal, Late Pubertal, and Adult.

Demographics can be seen in Tables 2.1 – 2.3. Figures 2.2(A) and 2.2(B) show a statistical difference between μ_a and μ_s' between sexes, but when broken down by age in Figures 2.2(C) and 2.2(D), late pubertal and adults have similar μ_a and μ_s' where as early pubertal subjects have different optical properties. The sex-age graphs in Figure 2.2(E) and

2.2(F) offer the most information about our subjects by showing two distinct groups. Late pubertal boys and adult males have similar μ_s' and μ_a spectra whereas early pubertal boys and all female participants have similar optical properties. This can be attributed to the increase in lean muscle mass seen in the transition from early to late pubertal boys without the increase in fat mass seen in late pubertal girls (Soliman et al 2014). When BMI is used to separate into normal, overweight and underweight groups, optical properties between groupings are shown to have no statistical difference in scattering or absorption spectra.

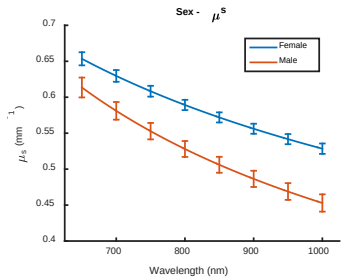

A

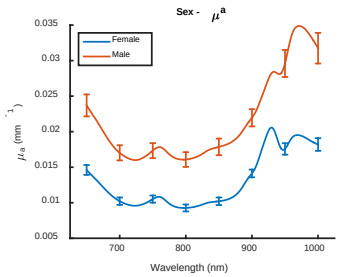

B

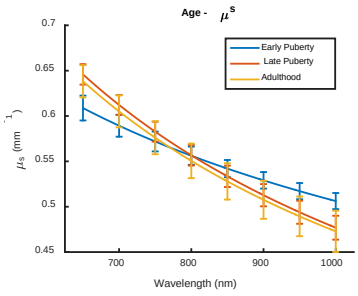

C

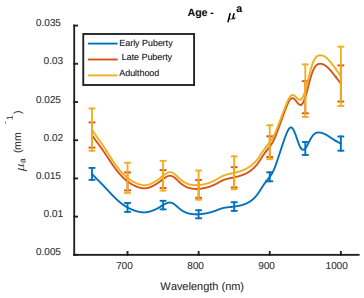

D

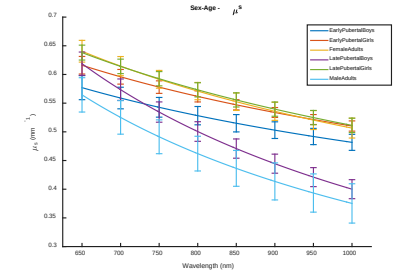

E

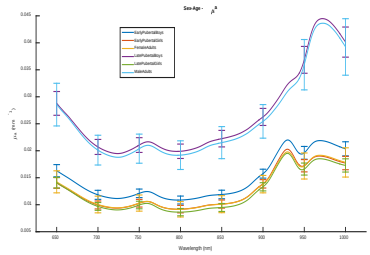

F

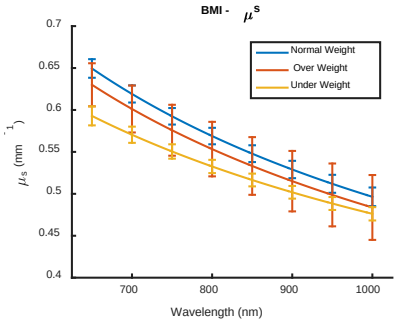

G

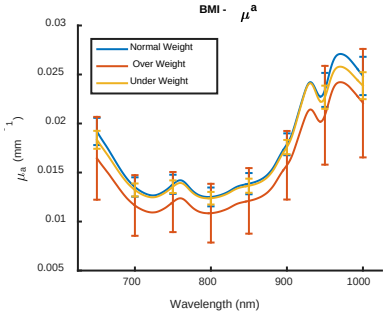

H

Figure 2.2 (A-H) – DOSI Scattering and Absorption Spectra of Participants grouped by Sex, Age, Sex-Age, and BMI. Standard Error of each category is plotted in the form of error bars.

DXA Body Fat vs DOSI

Having both DOSI parameters and DXA body fat percentage for these patients allowed for a direct comparison of DOSI to DXA for each body part and parameter to whole body fat percentage. Figure 2.3 has these comparison plots for each body part's total hemoglobin concentration.

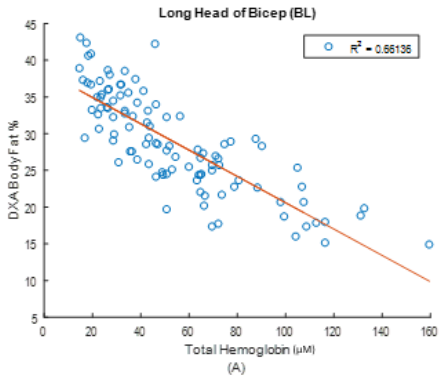
Long Head of Bicep (BL)
R² = 0.66136
DXA Body Fat %
Total Hemoglobin (μM)
(A)

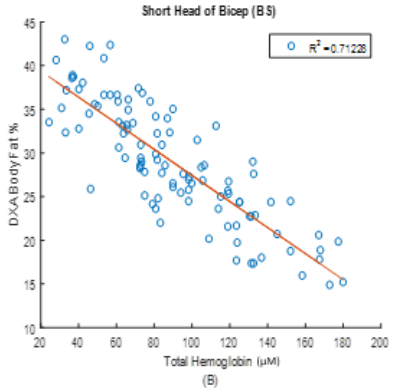
Short Head of Bicep (BS)
R² = 0.71228
DXA Body Fat %
Total Hemoglobin (μM)
(B)

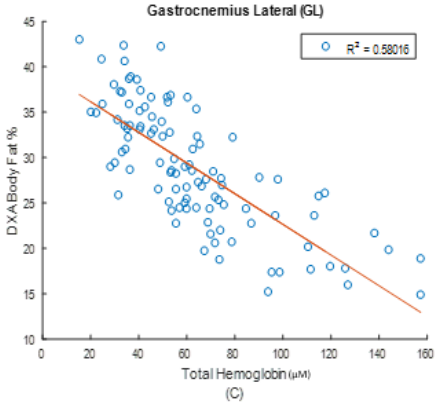
Gastrocnemius Lateral (GL)
R² = 0.58016
DXA Body Fat %
Total Hemoglobin (μM)
(C)

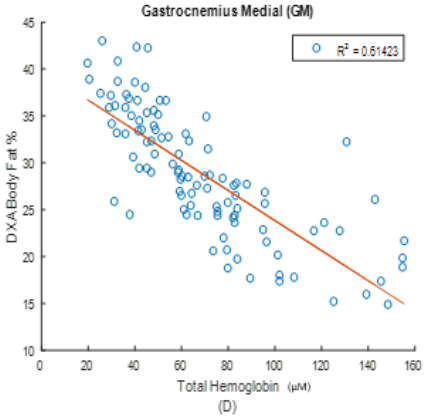
Gastrocnemius Medial (GM)
R² = 0.61423
DXA Body Fat %
Total Hemoglobin (μM)
(D)

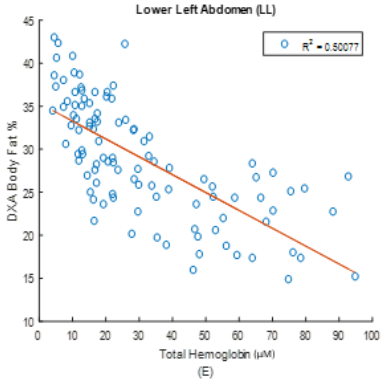
Lower Left Abdomen (LL)
R² = 0.50077
DXA Body Fat %
Total Hemoglobin (μM)
(E)

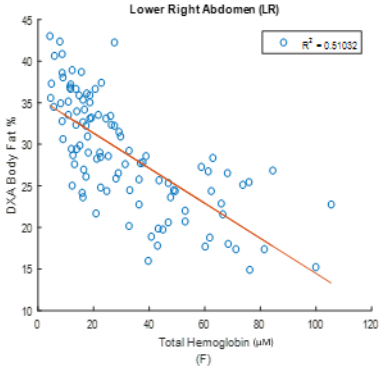
Lower Right Abdomen (LR)
R² = 0.51032
DXA Body Fat %
Total Hemoglobin (μM)
(F)

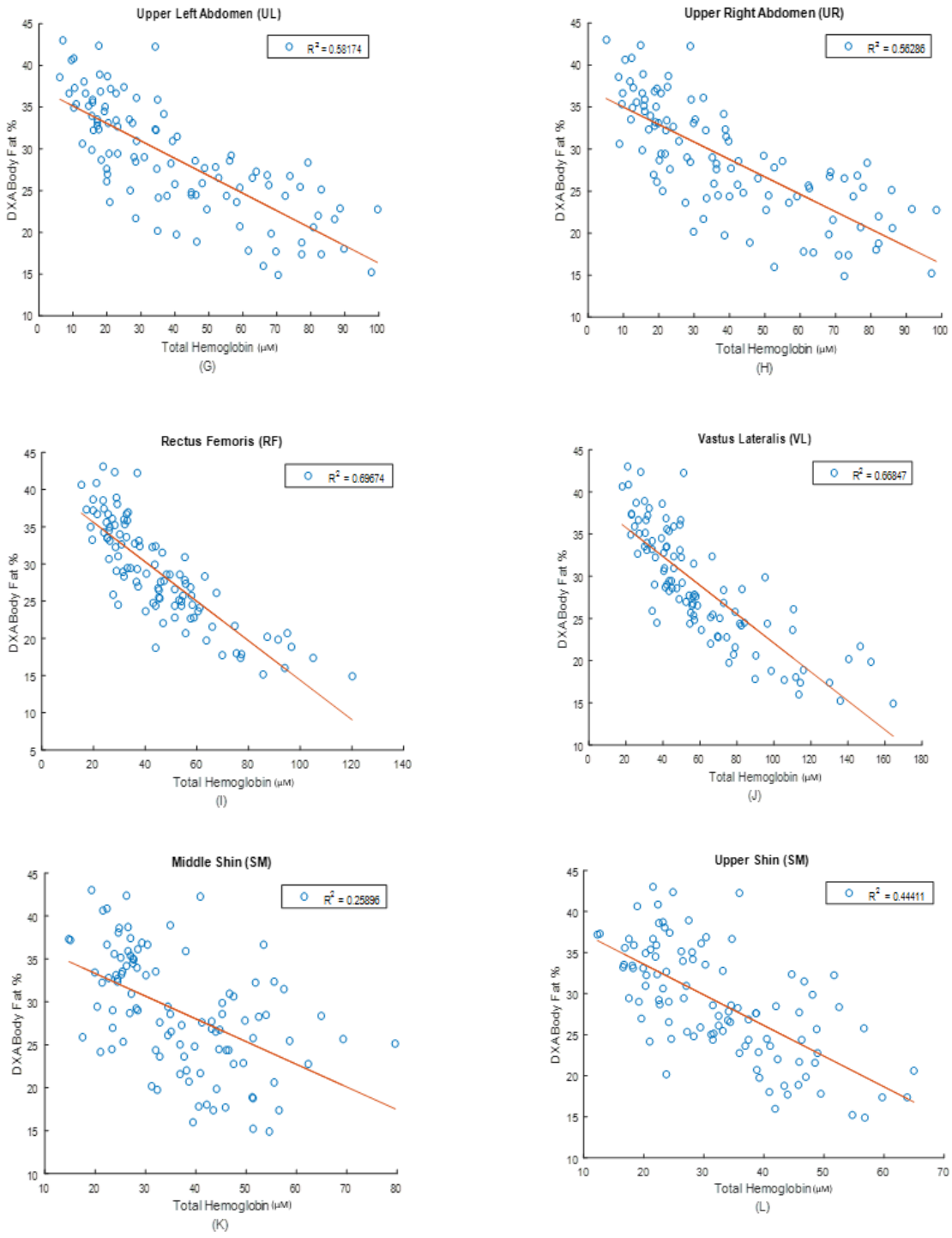

Figure 2.3(A-L) – Comparison of DOSI Total Hemoglobin Chromophore to DXA Body Fat % by body part.

Now that we have established that DOSI measurements throughout the body have a high correlation with DXA body fat percentage, a predictive model using DOSI parameters to predict body fat percentage can be made.

Predicting Body Fat with DOSI

To use DOSI parameters to predict body fat percentage, a linear model was selected to be the most effective method. We selected five DOSI parameters as possible predictive values at all twelve measurement sites. These parameters were THbMb, Water %, Fat %, A_s, and b_s. A correlation test was run on all 60 variables against DXA body fat percentage to determine if each measurement would be a good predictor. After applying a Holm-Bonferroni correction to correct for multiple comparison, Scattering Amplitude was shown to be a non-significant predictor of body fat percentage.

The next step was to construct a linear model using our four significant DOSI parameters to predict body fat percentage using Equation 2.1. Using THbMb, Water, Fat, and b_s, we designed a linear regression model to predict body fat percentage. Twenty percent of our patients were randomly excluded to test our model with once it was complete. The initial model used the four DOSI parameters from all twelve body location measurements. Each parameter was normalized to its entire set to reduce computational cost and increase efficiency. After normalization, the DOSI parameters were mapped to DXA body fat percentage using a gradient descent algorithm, the results of which can be seen in Table 2.4.

Equation 2.1 – Linear Model Form

$$Y_n = \beta_0 + \beta_1(X_{n1}) + \beta_2(X_{n2}) + \beta_3(X_{n3}) + \beta_4(X_{n4}) + \beta_5(X_{n5}) + \varepsilon_n$$

Table 2.4 – Initial Linear Model developed using DOSI parameters and DXA body fat percentage.

	Estimate	Std.Error	T value	Pr
Intercept	28.8537	0.2918	98.8858	0.000E+00
THBMB	-2.7063	0.9805	-2.7602	7.217E-03
Water	-0.9936	1.4927	-0.6656	5.076E-01
Fat	3.4416	1.2282	2.8022	6.417E-03
ScatB	-1.3376	0.4862	-2.7513	7.397E-03
Sample Size:		82		
RMSE:		2.54		
R squared:		0.86		
Adjusted R squared:		0.85		

To try to improve the model and reduce the number of measurements needed, a method for determining which sites provided the most important data to the model was created. First, each measurement site was fitted to the DXA body fat values, creating a new linear model. The body part with the highest adjusted R^2 was selected and saved (Bicep Short). Next, that site along with each other site was again fitted to DXA values, and the model with the highest adjusted R^2 was again saved (Bicep Short and Rectus Femoris). This process was repeated until the adjusted R^2 of the model stopped increasing. The

Table 2.5 – Correlation tests between our three DOSI chromophore parameters. High correlation between all three explains why one of the parameters has an insignificant p – value in the linear regression model.

Correlation Variables	R	P
Total Hemoglobin vs Water	-0.9435	2.8813e-50
Total Hemoglobin vs Fat	0.9616	1.5648e-58
Water vs Fat	-0.9692	2.9318e-63

final model can be seen in Table 2.6. The measurement sites selected were Bicep Short, Rectus Femoris, Lower Right Abdomen, Gastrocnemius Lateral, Upper Left Abdomen, and Vastus Lateralis. For both models, one can notice that the P – values for either water or fat say that those measurements are not statistically significant contributors to the model. However, the high p – values are due to high correlation between these parameters and other DOSI parameters used in the model (Table 2.5).

Table 2.6 – Final Linear Model comprised of DOSI measurements from Bicep Short, Rectus Femoris, Lower Right Abdomen, Gastrocnemius Lateral, Upper Left Abdomen, and Vastus Lateralis.

	Estimate	Std.Error	T value	Pr
Intercept	28.8270	0.2739	105.2275	0.000E+00
THBMB	-3.8778	1.0318	-3.7582	3.312E-04
Water	2.2793	1.1308	2.0157	4.732E-02
Fat	-1.2916	1.4654	-0.8814	3.809E-01
ScatB	-1.6549	0.4755	-3.4806	8.271E-04
Sample Size:		82		
RMSE:		2.39		
R squared:		0.88		
Adjusted R squared:		0.87		

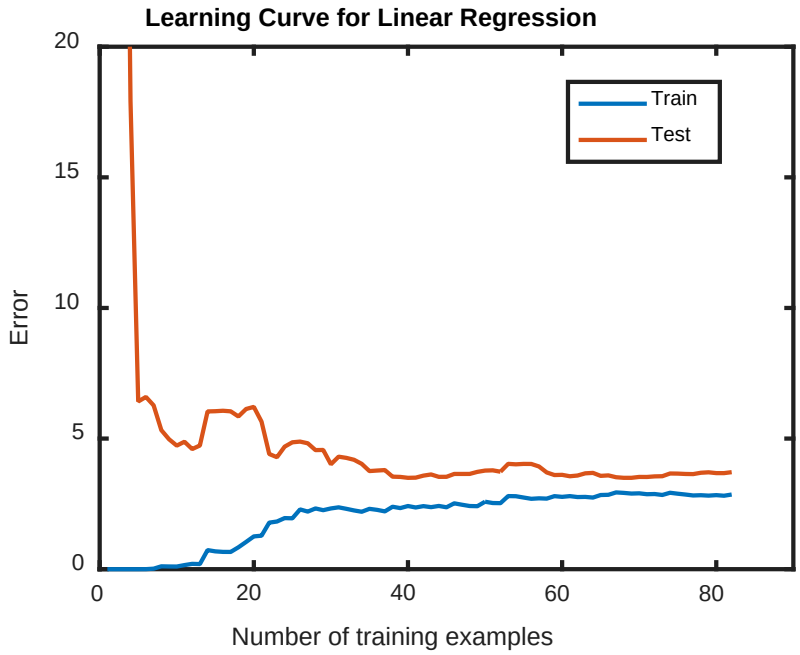

Figure 2.4 – Learning Curve for our final linear regression model. The Training and Test Errors converge to 3.29 %.

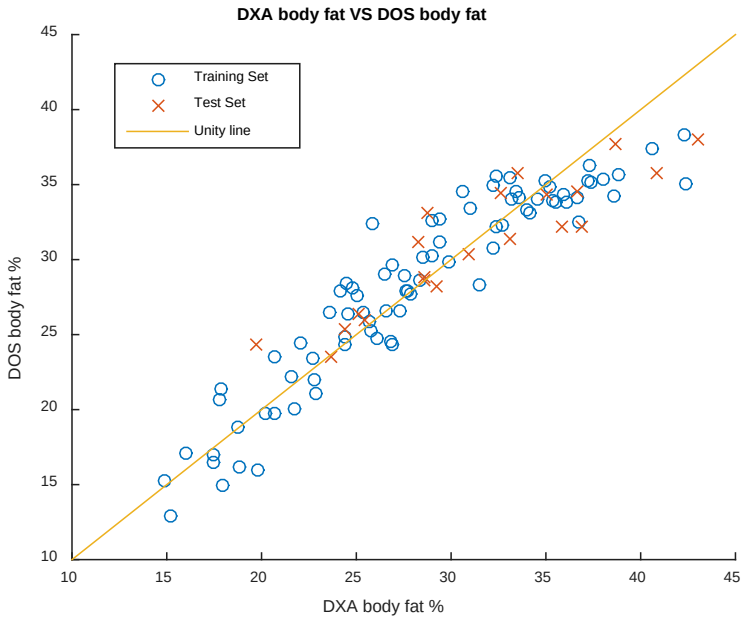

Figure 2.5 – Scatter Plot showing DXA body fat values vs DOSI body fat values. Unity line is plotted for reference. There is a high linearity between the two methods ($R^2 = 0.87$).

The full power of using the linear model can be seen in Figure 2.5. The high linearity between DXA body fat percentage, a gold standard for body composition measurements, and the DOSI body fat percentage linear model described above. With high correlation and low error, it is clear that DOSI is a useful tool for evaluating body fat percentage.

CHAPTER 3: Tissue Hydration Index

To evaluate the feasibility of creating an index from lipid and water measurements to predict water and fat, an initial test was performed between a ratio of water and fat DOSI parameters, and water and fat in Figure 3.1. Here, the Broadband Tissue Hydration Index (THI_{BB}) is first introduced and described by Equation 3.1. There is linear relationship between water and fat, and THI_{BB}. In Figure 3.1, as THI_{BB} increases, water increases, and fat decreases. The broadening at high THI_{BB} values on the water plot is due to other elements in the measurement volume that DOSI is not capable of quantifying (i.e. bone).

Equation 3.1 – Broadband Tissue Hydration Index

$$THI_{BB} = \frac{Water_{DOSI}}{Water_{DOSI} + Fat_{DOSI}}$$

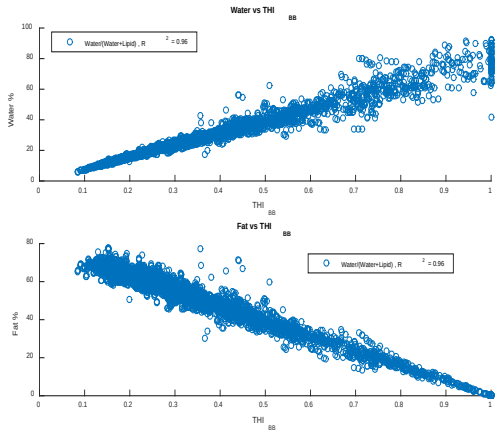

Figure 3.1 – Plots showing that there is a high correlation between DOSI Water and Fat chromophore concentrations and a ratio of them.

Wavelength Selection

Using the body composition data, we set about selecting the ideal wavelengths for a simplified two wavelength measurement system for fat and water concentration. Due to the shape of the absorption spectra, we selected a range of interest for lipid from 920nm to 940nm and a range of interest for water from 960nm to 980nm. The algorithm searched these ranges to find the minimum reflectance value, corresponding to a maximum in absorption

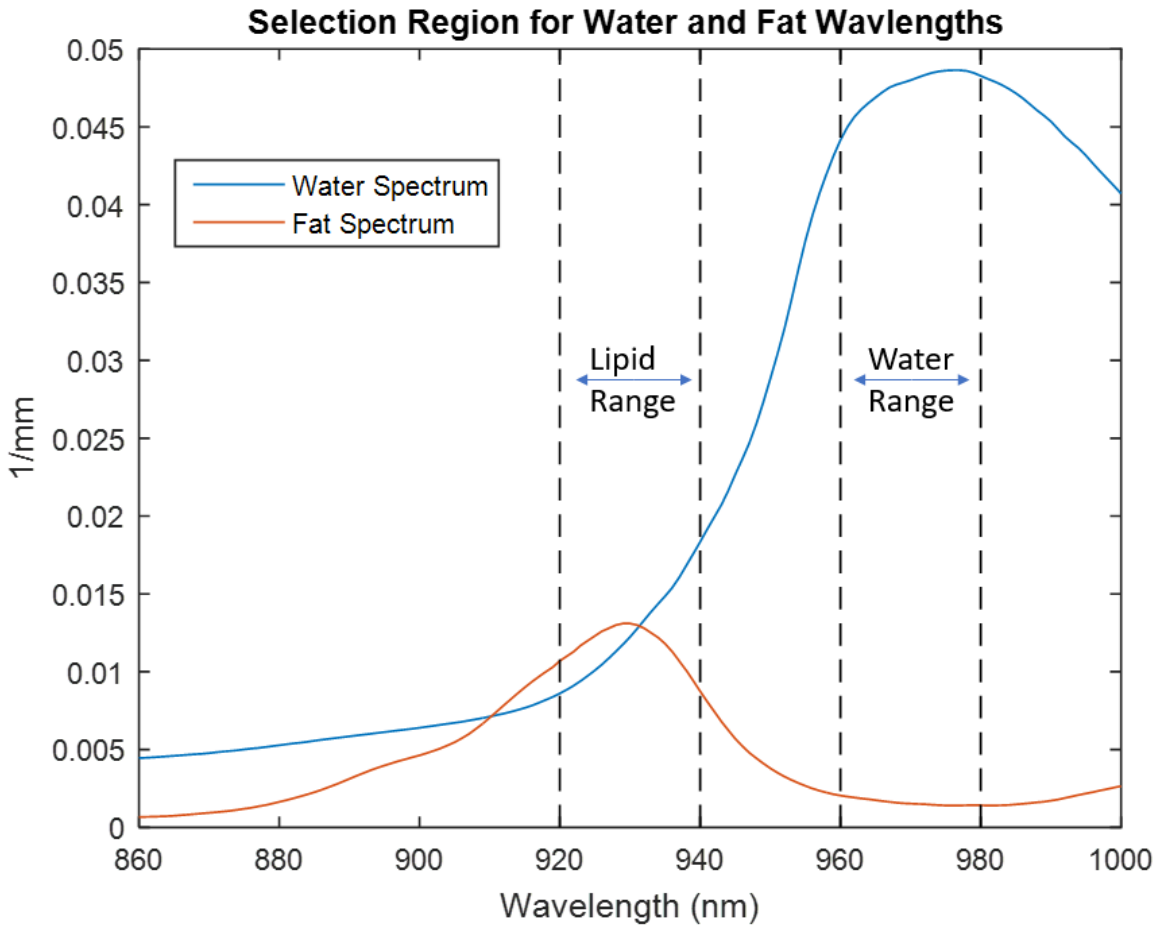

Figure 3.2 – Absorption Spectra of Lipid, Water, and ranges used for searching for lipid and water peaks for each measurement in the body composition data.

From the Figure 3.3, 969 nm was chosen as the optimal wavelength for the water diode and 929 nm was chosen as the optimal wavelength for the lipid diode. These measurements were taken from the steady state (SS) reflectance portion of the body composition data that was discussed previously in Chapter 2.

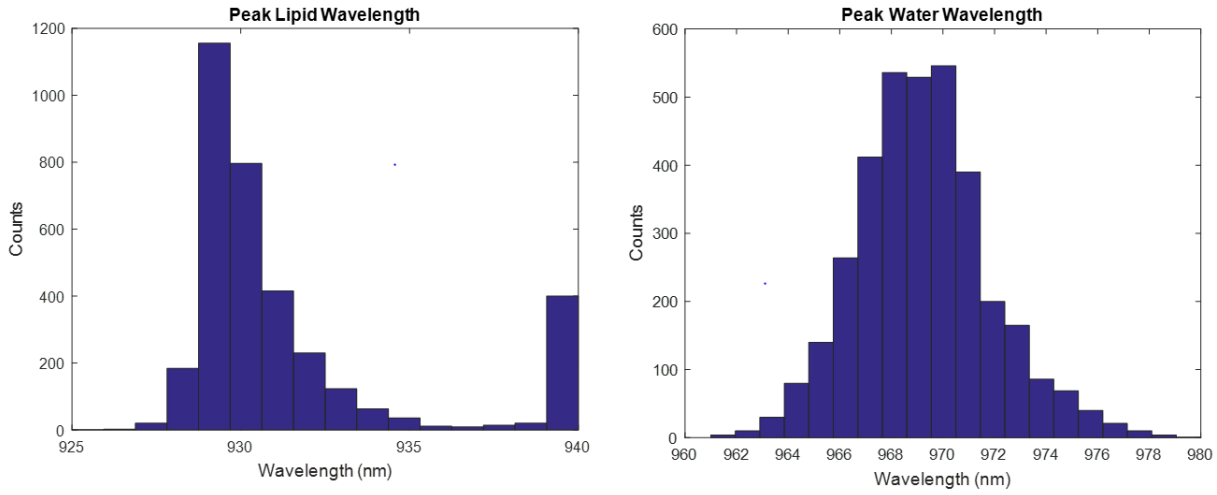

Figure 3.3 – Results of experiment described in previous figure. 929 nm was chosen as the wavelength to measure the lipid peak and 969 nm was chosen to measure the water peak. The column at 940 nm in the lipid histogram is due to participants with low fat content, thus having no discernible fat peak in their lipid spectra.

With the goal of replacing the spectrometer with just two laser diodes, LEDs or similar light sources, the reflectance measurements at 929 nm and 969 were used to create a lookup table to map Hydration to Water and Fat concentrations. For each patient, the calibrated reflectance values at these two wavelengths was taken and transformed into a measurement analogous to absorption by the equation 3.1 (Conway et al. 1984). This data is taken before the reflectance is adjusted by the theoretical value calculated by DOSI. The absorbance analog is then converted to the Steady State Tissue Hydration Index (THI_{SS}) using equation 3.2. To map THI_{SS} to Water % and Fat %, a lookup table was developed using water and fat concentrations from the DOSI body composition study.

Equation 3.1 – Absorbance analog transformation

$$\text{Absorbance}_{\text{analog}} = -\log_{10}(\text{Reflectance})$$

Equation 3.2 – Steady State Tissue Hydration Index

$$\text{THI}_{\text{SS}} = \frac{\text{Absorbance}_{\text{Water Peak}}}{\text{Absorbance}_{\text{Water Peak}} + \text{Absotrbance}_{\text{Lipid Peak}}}$$

As an initial test, Steady State reflectance data at 929nm and 969nm were calibrated using a reflectance standard, and transformed into absorbance, and then THI_{SS}. In Figure 3.4, there is a clear trend where change in slope increases with THI_{SS}. Because of this, a polynomial fit was selected to fit the data. The reverse trend in low THI_{SS} sections of the graphs (0.2 to 0.3) is inconsequential because we do not observe THI_{SS} values that low in our subjects.

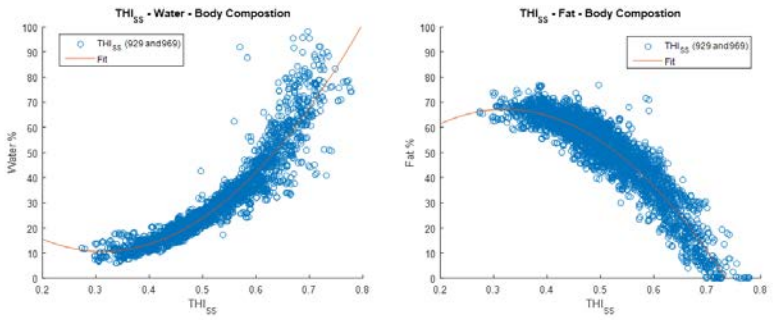

Figure 3.4 – Graphs of THI_{SS} vs Water and Fat Percentage. THI_{SS} is not linear, but can be modelled as a parable and adds the ability to quickly acquire data.

Validation

To assess how well the THI_{SS} performed in reality, several phantoms were made using different concentrations of Water and Fat and measured with DOSI. The THI_{SS} for

these phantoms were calculated and correlation tests and plots were made and are shown in Figure 3.4. The five high water, low fat phantoms were made by taking 20% intralipid and measuring it at stock solution concentration, and decreasing the fat concentration by 5% each time until only 1% fat remained (i.e. 20%, 15%, 10%, 5%, 1%). The medium water, medium fat phantoms, are just cheddar and cream cheese. Water concentrations were determined after DOS measurement by weighing the cheese before and after dehydration at 200°C for 6 hours. Fat concentrations were determined using the Total Fat and Serving Size information located on the packaging. For the low water, high fat phantoms, butter and lard were used. The water concentrations were determined by weighing the butter before and after heating on a hotplate for 30 minutes at 150°C. Both butter and lard fat measurements were taken from Total Fat and Serving Size information located on the packaging as well.

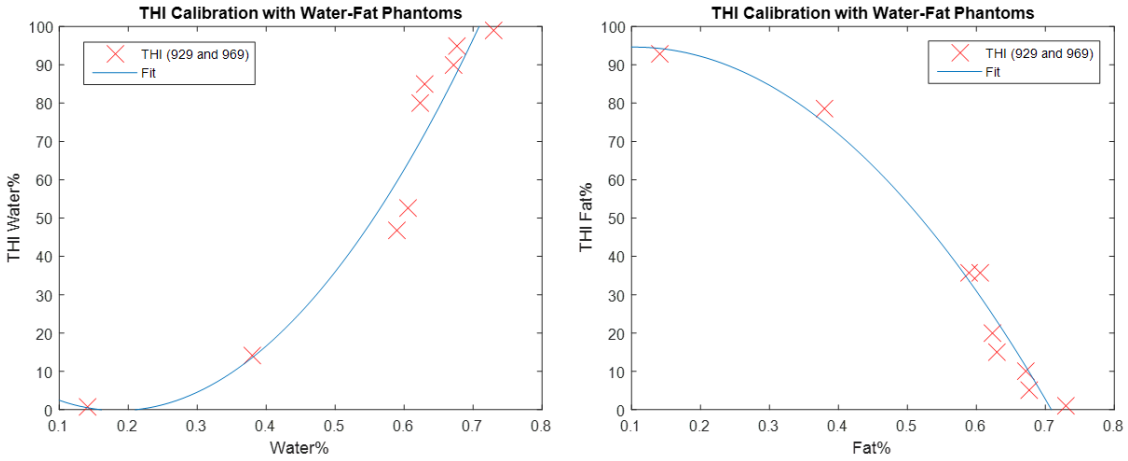

Figure 3.5 – Scatter plot showing Water % and Fat % vs THI_{SS}. There is a high correlation between both Water measurements and both Fat measurements. A unity line is shown to give a sense of the accuracy of these measurements.

Chapter 4: Summary and Conclusions

This paper presents three distinct yet related ideas. Using a study with a unique age range, we report on how differences in age, sex, age-sex category, and BMI can impact tissue scattering and absorption spectra. The difference between sexes can be distinguished in late pubertal and adult subjects, but not in early pubertal. Scattering and Absorption spectra offer no clear difference between the BMI categories of normal, overweight and underweight subjects.

After seeing that there was a high correlation between DXA body fat percentage and DOSI parameters, a linear model was made to map DOSI total hemoglobin, water, fat, and scattering power to DXA body fat percentage. This resulting model was validated by excluding 20% of our data from the training data and evaluating the model error on the test data.

Finally, a Tissue Hydration Index is introduced for the first time. Initial tests using broadband DOSI, followed by wavelength optimization using only 2 steady state (SS) reflectance wavelengths, resulted in the THI_{SS} being evaluated at 929nm for the lipid peak and 969nm for the water peak. To test the validity of the THI, phantoms with varying water and fat were made and those concentrations were plotted against the THI_{SS} to make a titration curve, showing the predictive power of the THI_{SS}.

Future Work

There are several paths for this work to be taken. Measurements of obese subjects, as well as elite athletes to further characterize DOSI's predictive power as it comes to body composition. To further study lean soft tissue, or muscle, comparing DOSI to MRI instead of

DXA would be preferable because MRI can quantify muscle better than DXA. To take full advantage of DOSI, hemodynamic measurements for each patient would allow for DOSI to be used a risk assessment method for disease. And to get a full view of the overall population, expanding the age range to 35 and older would provide more information on the overall population.

To further the THI_{SS}, constructing a standalone system that uses continuous wave lasers, LEDs, or conventional light sources at 929nm and 969nm, or similar wavelengths, would be a good step in showing the power of the THI_{SS} to predict water and fat percentage using a lookup table. THI_{BB} and THI_{SS} could be used to monitor hydration states of tissue during exercise,

References

Bevilacqua, F., Berger, A. J., Cerussi, A. E., Jakubowski, D., & Tromberg, B. J. (2000). Broadband absorption spectroscopy in turbid media by combined frequency-domain and steady-state methods. Applied Optics, 39(34), 6498. doi:10.1364/ao.39.006498

Conway, J. M., Norris, K. H., & Bodwell, C. E. (1984, December). A new approach for the estimation of body composition: infrared interactance. Retrieved from https://www.ncbi.nlm.nih.gov/pubmed/6507337

Elwell, C. E., & Kolyva, C. (2011). Making light work: illuminating the future of biomedical optics. Philosophical Transactions of the Royal Society A: Mathematical, Physical and Engineering Sciences, 369(1955), 4355-4357. doi:10.1098/rsta.2011.0303

Ganesan, G., Warren, R. V., Leproux, A., Compton, M., Cutler, K., Wittkopp, S., … Tromberg, B. J. (2016). Diffuse optical spectroscopic imaging of subcutaneous adipose tissue metabolic changes during weight loss. International Journal of Obesity (2005), 40(8), 1292–1300. http://doi.org/10.1038/ijo.2016.43

Ganesan, G., Cotter, J. A., Reuland, W., Cerussi, A. E., Tromberg, B. J., & Galassetti, P. (2015). Effect of Blood Flow Restriction on Tissue Oxygenation during Knee Extension. Medicine and Science in Sports and Exercise, 47(1), 185–193. http://doi.org/10.1249/MSS.0000000000000393

Lavie, C. J., Milani, R. V., & Ventura, H.O., (2009). Obesity and Cardiovascular Disease: Risk Factor, Paradox, and Impact of Weight Loss. Journal of the American College of Cardiology, 53(21),1925-32. doi:10.1016/j.jacc.2008.12.068.

Lee, J., Saltzman, D. J., Cerussi, A. E., Gelfand, D. V., Milliken, J., Waddington, T., . . . Brenner, M. (2006). Broadband diffuse optical spectroscopy measurement of hemoglobin concentration during hypovolemia in rabbits. Physiological Measurement, 27(8), 757-767. doi:10.1088/0967-3334/27/8/009

Ng, M., Fleming, T., Robinson, M., Thomson, B., Graetz, N., … Gakidou, E. (2014). Global, regional and national prevalence of overweight and obesity in children and adults 1980-2013: A systematic analysis. Lancet (London, England), 384(9945), 766–781. http://doi.org/10.1016/S0140-6736(14)60460-8

O'Sullivan, T. D., Leproux, A., Chen, J.-H., Bahri, S., Matlock, A., Roblyer, D., … Tromberg, B. J. (2013). Optical imaging correlates with magnetic resonance imaging breast density and reveals composition changes during neoadjuvant chemotherapy. Breast Cancer Research: BCR, 15(1), R14. http://doi.org/10.1186/bcr3389

Pham, T. H., Hornung, R., Ha, H. P., Burney, T., Serna, D., Powell, L., . . . Tromberg, B. J. (2002). Noninvasive monitoring of hemodynamic stress using quantitative near-infrared frequency-domain photon migration spectroscopy. Journal of Biomedical Optics, 7(1), 34. doi:10.1117/1.1427046

Popowski, L. A., Oppliger, R. A., Lambert, G. P., Johnson, R. F., Johnson, A. K., & Gisolfi, C. V. (2001). Blood and urinary measures of hydration status during progressive acute dehydration. Medicine and Science in Sports and Exercise, 747-753. doi:10.1097/00005768-200105000-00011

Soliman, A., De Sanctis, V., & Elalaily, R. (2014). Nutrition and pubertal development. Indian Journal of Endocrinology and Metabolism, 18(Suppl 1), S39–S47. http://doi.org/10.4103/2230-8210.145073